



# Nonlinear analysis of functionally graded nanocomposite rotating thick disks with variable thickness reinforced with carbon nanotubes



Hassan Zafarmand, Mehran Kadkhodayan\*

Department of Mechanical Engineering, Ferdowsi University of Mashhad, Mashhad 91775-1111, Iran

## ARTICLE INFO

### Article history:

Received 13 January 2014

Received in revised form 10 June 2014

Accepted 15 December 2014

Available online 23 December 2014

### Keywords:

Nonlinear analysis

Carbon nanotube

Functionally graded materials

Thick rotating disk

Variable thickness

Nonlinear graded finite element method

## ABSTRACT

In this paper the nonlinear elasticity solution of functionally graded nanocomposite rotating thick disks with variable thickness reinforced with single-walled carbon nanotubes (SWCNTs) is presented. Four distribution types of uniaxial aligned SWCNTs are considered: uniform and three types of functionally graded (FG) distributions along radial direction of the disk. The effective material properties of the nanocomposite disk are estimated by a micro-mechanical model. The governing nonlinear equations are based on the axisymmetric theory of elasticity with the geometric nonlinearity in axisymmetric complete form. The nonlinear graded finite element method (NGFEM) based on Rayleigh–Ritz energy formulation with the Picard iterative scheme is employed to solve the nonlinear equations. The solution is considered for four different thickness profiles, namely constant, linear, concave and convex. The effects of different types of distributions and volume fractions of CNTs and various types of thickness profiles on the displacement and stresses of the rotating disks as well as comparison between linear and nonlinear responses are investigated. The achieved results show that the displacement and stress fields can be controlled by changing the type of distribution and volume fraction of CNTs as well as the thickness profile. Moreover, the difference between linear and nonlinear results are noticeable in high angular velocities; thus, for obtaining accurate results, the geometric nonlinearity must be considered.

© 2014 Elsevier Masson SAS. All rights reserved.

## 1. Introduction

Rotating disks are of practical concern in many fields of engineering, such as marine, mechanical and aerospace industry including gas turbines, gears, turbo-machinery, flywheel systems and centrifugal compressors. The stresses due to centrifugal load can have important effects on their strength and safety. Thus, control and optimization of stress and displacement fields can help to reduce the overall payload in aerospace industry.

In recent years, nano-structured materials such as nanocomposites have generated considerable interest in the material research community and became an attractive new subject in material science due to their potentially impressive mechanical properties. Carbon nanotubes (CNTs) have illustrated remarkable mechanical, thermal and electrical properties. For instance, they could potentially have a Young's modulus as high as 1 TPa and a tensile strength approaching 100 GPa [20]. These enormous advantages make them highly desirable candidates for the reinforcement of the polymer composites, provided that good interfacial bonding

between CNTs and polymer and proper dispersion of the individual CNTs in the polymeric matrix can be assured [9].

The majority of researches performed on carbon nanotube reinforced composites (CNTRCs) are focused on their material properties [8,29,6,13,17]. Han and Elliott [11] by use of molecular dynamic simulation (MD) obtained the elastic modulus of composite structures reinforced with CNTs and studied the effect of volume fraction of SWCNTs on mechanical properties of nanocomposites. Hu et al. [12] by analyzing the elastic deformation of a representative volume element (RVE) under various loading conditions evaluated the macroscopic elastic properties of CNTRCs. Zhu et al. [36] studied the effect of CNTs on the mechanical properties of polymeric composites. Their results show that adding CNTs can greatly improve the Young's modulus. Due to dependency of the interaction at the polymer and nanotube interface on the local molecular structure and bonding, Odegard et al. [21], by utilizing an equivalent-continuum modeling method, proposed a constitutive model for CNTRCs.

Functionally graded materials (FGMs) are special composite materials, microscopically inhomogeneous, in which the mechanical properties vary smoothly and continuously from one surface to the other. This idea which was used for the first time by Japanese researchers [15], leads to the concept of FGMs. A wide range of

\* Corresponding author. Tel.: +0098 9153111869.

E-mail address: kadkhoda@um.ac.ir (M. Kadkhodayan).

researches have been carried out on FGMs in various fields of mechanics. Motivated by the concept of FGMs, Shen [26] presented a type of CNTRCs that the volume fraction of CNTs are graded with certain rules along desired directions and demonstrated that the use of FG-CNTRCs improves the mechanical properties of the structures. Zhu et al. [35] studied the bending and free vibration analyses of composite plates reinforced with SWCNTs using the finite element method based on the first order shear deformation plate theory. The effective material properties of the FG-CNTRC are graded in the thickness direction and are estimated according to the rule of mixtures. The three-dimensional free vibration of FC-CNTRC panels has been investigated by Yas et al. [30]. The boundary conditions are assumed to be simply support and the equations are solved by a generalized differential quadrature (GDQ) method. Shen [27] presented a postbuckling analysis for nanocomposite cylindrical shells reinforced with single-walled carbon nanotubes (SWCNTs) subjected to lateral or hydrostatic pressure in thermal environments. Sobhani Aragh and Yas [28] investigated the static and free vibration characteristics of continuously graded fiber-reinforced (CGFR) cylindrical shells based on three-dimensional theory of elasticity. The boundary conditions are assumed to be simply support and the equations are solved by a GDQ method. Moradi-Dastjerdi et al. [18] studied the free vibration of FG-CNTRC cylinders with a mesh-free method. The conditions are assumed to be axisymmetric where the effect of the waviness of the CNTs and its parameters are studied.

Moreover, numerous researches have been performed on analysis of functionally graded rotating disks. Durodola and Attia [7] studied the deformation and stress fields in functionally graded rotating disks using direct numerical integration of the governing differential equations as well as finite element analysis. Zenkour [33] investigated an analytical solution for functionally graded annular rotating disks under the plane-stress assumption with exponentially variable material properties. He later extended this solution to a variable thickness rotating disk [34]. Nie and Batra [19] obtained the equation of functionally graded rotating disks with variable thickness by using an Airy stress function and solved both analytically and numerically using the differential quadrature method. Kordkheili and Naghdabadi [16] presented a semi-analytical thermoelasticity solution for hollow and solid rotating axisymmetric disks made of functionally graded materials based on the plane-stress assumption. Their solution is based on dividing the radial domain into sub-domains. Callioğlu et al. [5] investigated the stress analysis of functionally graded rotating disks and demonstrated that they have the capability of higher angular rotations compared with the homogeneous isotropic ones. Asghari and Ghafoori [1] proposed a semi-analytical three-dimensional elasticity solution for the rotating functionally graded problem suitable for thick disks. Zafarmand and Hassani [31] presented the elasticity solutions of 2D-FG thick rotating annular and solid disks with variable thickness. Shariyat and Mohammadjani [25] studied the stress analysis of rotating thick 2D-FG annular plates with non-uniform loads and elastic foundation. A second order point collocation method with forward-backward schemes was adopted to solve the system of the governing and boundary conditions.

According to literature, the studies deal with linear analysis of rotating disks. It has to be noted that in high speed advanced modern technologies such as gas turbines, turbochargers, centrifugal devices or machine tools, the speeds of rotary parts may approach up to  $\omega = 20000$  rad/s. Thus, the application of linear analysis to high angular velocities may cause remarkable errors. Therefore, in order to obtain accurate results, the nonlinear analysis should be applied. Very few nonlinear analysis have been presented so far for rotating disks [10,3], in which their governing nonlinear equations are based on plate theories with von Karman large displacement scheme that do not involve nonlinear terms of radial displacement.

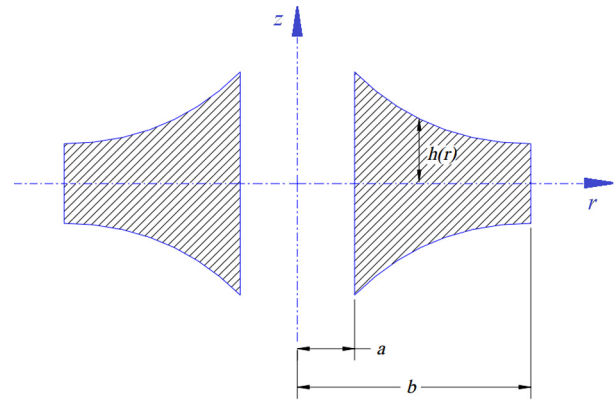


Fig. 1. Axisymmetric thick FG-CNTRC rotating disk.

To the best knowledge of the authors, there are no studies available in the literature on nonlinear analysis of FG-CNTRC rotating disks with variable thickness based on elasticity theory with the geometric nonlinearity in axisymmetric complete form. Thus, the purpose of this paper is to investigate the nonlinear analysis of thick FG-CNTRC rotating disks with variable thickness. Material properties are assumed to vary continuously along radial direction. The effective material properties of FG-CNTRC disk are estimated using a micro-mechanical model and the displacement and stress fields of FG-CNTRC disk for various types of distributions and volume fractions of CNTs as well as different types of thickness profiles are computed and compared. The difficulty in obtaining analytical solutions for the response of graded material systems comes from the dispersion of the heterogeneous material systems. Therefore, analytical or semi-analytical solutions are available only through a number of problems with simple boundary conditions. Besides, in the case of nonlinear analysis, the availability of such solutions becomes narrower. Thus, in order to find the nonlinear solution for a thick FG-CNTRC disk with variable thickness, powerful numerical methods such as nonlinear graded finite element method (NGFEM) are needed. The graded finite element incorporates the gradient of the material properties at the element scale in the framework of a generalized isoparametric formulation. Some studies can be found in the literature on modeling of non-homogeneous structures by using GFEM [14,2,32]. In these studies, it is shown that the conventional FEM formulation causes a discontinuous stress field whereas the graded elements give a continuous and smooth variation.

## 2. Problem formulation

In this section different types of CNTs' distributions along radial direction of the disk are investigated. The axisymmetric governing nonlinear equations of motion are obtained and nonlinear graded finite element method is employed for modeling the material non-homogeneity and geometric nonlinearity.

### 2.1. Material properties in FG-CNTRC rotating disk

A thick FG-CNTRC disk of inner radius  $a$ , outer radius  $b$  and variable thickness  $h(r)$  is considered. The geometry and coordinate system of the disk is shown in Fig. 1.

This FG-CNTRC disk consists of radially aligned SWCNTs and an isotropic matrix. Several studies have been published each with different focuses on mechanical properties of CNTRCs. However, for the sake of simplicity in the present study the rule of mixtures is employed and thus the effective material properties of CNTRC disk can be obtained as [26]:

**Table 1**  
Comparison of Young's moduli for polymer/CNTRC at  $T_0 = 300$  [30].

$V_{CNT}^*$	MD [11]		Extended rule of mixtures			
	$E_1$ (GPa)	$E_2$ (GPa)	$E_1$ (GPa)	$\eta_1$	$E_2$ (GPa)	$\eta_2$
0.12	94.6	2.9	94.78	0.137	2.9	1.022
0.17	138.9	4.9	138.68	0.142	4.9	1.626
0.28	224.2	5.5	224.5	0.141	5.5	1.585

$$E_1 = \eta_1 V_{CNT} E_1^{CNT} + V_m E^m \quad (1)$$

$$\frac{\eta_2}{E_i} = \frac{V_{CNT}}{E_i^{CNT}} + \frac{V_m}{E^m} \quad (i = 2, 3) \quad (2)$$

$$\frac{\eta_3}{G_{ij}} = \frac{V_{CNT}}{G_{ij}^{CNT}} + \frac{V_m}{G^m} \quad (i \neq j) \quad (3)$$

$$v_{ij} = V_{CNT} v_{ij}^{CNT} + V_m v^m \quad (i \neq j) \quad (4)$$

$$\rho = V_{CNT} \rho^{CNT} + V_m \rho^m \quad (5)$$

where  $E_i^{CNT}$ ,  $G_{ij}^{CNT}$ ,  $v_{ij}^{CNT}$  and  $\rho^{CNT}$  are elasticity modulus, shear modulus, Poisson's ratio and density respectively, of the CNTs and  $E^m$ ,  $G^m$ ,  $v^m$  and  $\rho^m$  are corresponding properties for the matrix.  $\eta_j$  ( $j = 1, 2, 3$ ) is the CNTs' efficiency parameter where its determination is a key issue for successful application of the extended rule of mixtures to CNTRCs. This parameter can be computed by matching the elastic modulus of CNTRCs observed from the MD simulation results with those obtained from rule of mixtures. Han and Elliott [11] with the use of MD simulation and energy minimization obtained the elastic moduli of polymer/CNT composites. In the conventional rule of mixtures the whole system is assumed to be continuum and the interfaces between the matrix and fibers remain fully intact, thus the general macroscopic rule of mixtures cannot be applied straightforwardly to composites with strong interfacial interactions. Besides, micromechanics equations cannot capture the scale difference between the nano and micro levels. For this purpose, CNT efficiency parameters  $\eta_j$  ( $j = 1, 2, 3$ ) are obtained by comparing the Young's moduli  $E_1^{CNT}$  and  $E_2^{CNT}$  of CNTRCs achieved from the extended rule of mixtures to those from MD simulation given by [11]. It should be noticed that there are no MD results available for shear modulus  $G_{12}$  in Ref. [11]. The results are shown in Table 1 and are used in the present study, in which it is assumed that  $\eta_3 = 0.7\eta_2$  [30].

Moreover,  $V_{CNT}$  and  $V_m$  are the volume fractions of the CNTs and matrix, respectively, which is assumed to be related by  $V_{CNT} + V_m = 1$ , this assumption comes from considering a perfect composite (no voids, etc.). It has to be stated that this assumption may yield results somewhat different from the experimental ones.

Furthermore, the volume fraction of CNTs ( $V_{CNT}$ ) is assumed to be graded continuously along the radial direction of the disk, hence, the disk is consisted of inhomogeneous and anisotropic material. Accordingly, four distribution types are defined in this study; that is either uniformly distributed (UD) or three types of functionally graded (FG\_V, FG\_O and FG\_X) in radial direction. They are assumed to be as [26]:

$$V_{CNT} = V_{CNT}^* \quad (\text{type UD}) \quad (6)$$

$$V_{CNT} = 2 \left( \frac{r-a}{b-a} \right) V_{CNT}^* \quad (\text{type FG}_V) \quad (7)$$

$$V_{CNT} = 2 \left( \frac{b-r}{b-a} \right) V_{CNT}^* \quad (\text{type FG}_O) \quad (8)$$

$$V_{CNT} = 4 \left| \frac{r-r_m}{b-a} \right| V_{CNT}^* \quad (\text{type FG}_X) \quad (9)$$

in which:

$$r_m = \left( \frac{a+b}{2} \right) \quad (10)$$

$$V_{CNT}^* = \frac{w_{CNT}}{w_{CNT} + (\rho_{CNT}/\rho_m) - (\rho_{CNT}/\rho_m)w_{CNT}} \quad (11)$$

where  $w_{CNT}$  is the mass fraction of CNTs,  $\rho_{CNT}$  and  $\rho_m$  are the densities of CNTs and matrix, respectively.

## 2.2. Governing equations

In the case of rotating disk, the body force is directed along the radial direction. Hence, the equations of equilibrium with the axisymmetric assumption in term of stresses are obtained as [4]:

$$\begin{aligned} \frac{\partial \sigma_r}{\partial r} + \frac{\partial \sigma_{rz}}{\partial z} + \frac{\sigma_r - \sigma_\theta}{r} + \rho r \omega^2 &= 0 \\ \frac{\partial \sigma_{rz}}{\partial r} + \frac{\partial \sigma_z}{\partial z} + \frac{\sigma_{rz}}{r} &= 0 \end{aligned} \quad (12)$$

where  $\rho$  is the mass density that can be a function of radial coordinate according to Eq. (5).

The stress-strain relation from the Hook's law in matrix form is as [24]:

$$\sigma = \mathbf{D} \epsilon \quad (13)$$

where the stress and strain components and the coefficients of elasticity  $\mathbf{D}$ , are as the following relations [24]:

$$\sigma = \{ \sigma_r \quad \sigma_\theta \quad \sigma_z \quad \sigma_{rz} \}^T \quad (14)$$

$$\epsilon = \{ \epsilon_r \quad \epsilon_\theta \quad \epsilon_z \quad \gamma_{rz} \}^T \quad (15)$$

$$\mathbf{D} = \begin{bmatrix} D_{11} & D_{12} & D_{13} & 0 \\ D_{12} & D_{22} & D_{23} & 0 \\ D_{13} & D_{23} & D_{33} & 0 \\ 0 & 0 & 0 & D_{55} \end{bmatrix} \quad (16)$$

in which:

$$\begin{aligned} D_{11} &= \frac{1 - \nu_{23}\nu_{32}}{E_2 E_3 \Delta}, & D_{22} &= \frac{1 - \nu_{13}\nu_{31}}{E_1 E_3 \Delta}, \\ D_{33} &= \frac{1 - \nu_{12}\nu_{21}}{E_1 E_2 \Delta}, & D_{12} &= \frac{\nu_{21} + \nu_{31}\nu_{23}}{E_2 E_3 \Delta}, \\ D_{13} &= \frac{\nu_{31} + \nu_{21}\nu_{32}}{E_2 E_3 \Delta}, & D_{23} &= \frac{\nu_{32} + \nu_{12}\nu_{31}}{E_1 E_3 \Delta}, \\ D_{55} &= G_{13}, \\ \Delta &= \frac{1 - \nu_{12}\nu_{21} - \nu_{23}\nu_{32} - \nu_{13}\nu_{31} - 2\nu_{21}\nu_{32}\nu_{13}}{E_1 E_2 E_3} \end{aligned} \quad (17)$$

where  $E_i$ ,  $G_{ij}$  and  $\nu_{ij}$  are found from Eqs. (1)–(4).

The strain-displacement equations based on the Green–Lagrange axisymmetric form in cylindrical coordinate are [4]:

$$\begin{aligned} \epsilon_r &= \frac{\partial u}{\partial r} + \frac{1}{2} \left[ \left( \frac{\partial u}{\partial r} \right)^2 + \left( \frac{\partial w}{\partial r} \right)^2 \right] \\ \epsilon_\theta &= \frac{u}{r} + \frac{1}{2} \left( \frac{u}{r} \right)^2 \\ \epsilon_z &= \frac{\partial w}{\partial z} + \frac{1}{2} \left[ \left( \frac{\partial u}{\partial z} \right)^2 + \left( \frac{\partial w}{\partial z} \right)^2 \right] \\ \gamma_{rz} &= \frac{\partial u}{\partial z} + \frac{\partial w}{\partial r} + \left[ \frac{\partial u}{\partial z} \frac{\partial u}{\partial r} + \frac{\partial w}{\partial z} \frac{\partial w}{\partial r} \right] \end{aligned} \quad (18)$$

where  $u$  and  $w$  are radial and axial components of displacement, respectively.

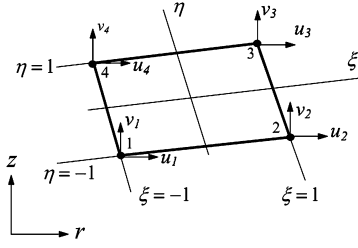


Fig. 2. Local coordinate.

### 2.3. Graded finite element modeling

In order to solve the governing nonlinear equations, the nonlinear graded finite element method is used. In this method, in addition to displacement field, the heterogeneity of the material properties of the FGM may also be determined based on their nodal values. In this regard, shape functions similar to those of the displacement fields may be used. Therefore, a graded finite element method (GFEM) is used to effectively trace smooth variations of the material properties at the element level. Using the graded elements for modeling of gradation of the material leads to more accurate results than dividing the solution domain into homogeneous elements.

The finite element approximation of the domain is in the  $r$ - $z$  plane, which is the plane of revolution. The section of the disk in the  $r$ - $z$  plane is considered and divided into a number of simplex linear quadrilateral elements. For convenience the local coordinate is used which its variables ( $\xi$ ,  $\eta$ ) are between  $-1$  to  $1$  as is shown in Fig. 2.

For element ( $e$ ), the displacements are approximated as [23]:

$$\mathbf{U}^{(e)} = \Phi \mathbf{A}^{(e)} \quad (19)$$

where  $\mathbf{U}^{(e)}$  is the element displacements vector,  $\Phi$  is the matrix of linear shape functions in local coordinate and  $\mathbf{A}^{(e)}$  is the element nodal displacement vector that are as:

$$\mathbf{U}^{(e)} = \begin{Bmatrix} u \\ w \end{Bmatrix}^{(e)} \quad (20)$$

$$\Phi = \begin{bmatrix} \Phi_1 & 0 & \Phi_2 & 0 & \Phi_3 & 0 & \Phi_4 & 0 \\ 0 & \Phi_1 & 0 & \Phi_2 & 0 & \Phi_3 & 0 & \Phi_4 \end{bmatrix} \quad (21)$$

$$\mathbf{A}^{(e)} = \{U_1 \quad V_1 \quad U_2 \quad V_2 \quad U_3 \quad V_3 \quad U_4 \quad V_4\}^T \quad (22)$$

in which:

$$\Phi_i = \frac{1}{4}(1 + \xi_i \xi)(1 + \eta_i \eta) \quad (23)$$

To treat the material inhomogeneity by using the GFEM, it may be written:

$$\Psi^{(e)} = \sum_{i=1}^4 \psi_i \Phi_i \quad (24)$$

where  $\Psi^{(e)}$  is the material property of the element.

Substituting Eq. (19) in Eq. (18) gives the element strain matrix as:

$$\boldsymbol{\varepsilon}^{(e)} = \underbrace{(\mathbf{B}_L + \mathbf{B}_{NL})}_{\mathbf{B}} \mathbf{A}^{(e)} \quad (25)$$

where:

$$\mathbf{B}_L = \begin{bmatrix} \frac{\partial \Phi_1}{\partial r} & 0 & \dots & \frac{\partial \Phi_4}{\partial r} & 0 \\ \frac{\Phi_1}{r} & 0 & \dots & \frac{\Phi_4}{r} & 0 \\ 0 & \frac{\partial \Phi_1}{\partial z} & \dots & 0 & \frac{\partial \Phi_4}{\partial z} \\ \frac{\partial \Phi_1}{\partial z} & \frac{\partial \Phi_1}{\partial r} & \dots & \frac{\partial \Phi_4}{\partial z} & \frac{\partial \Phi_4}{\partial r} \end{bmatrix}$$

$$\mathbf{B}_{NL} = \begin{bmatrix} \frac{1}{2}(\sum_{i=1}^4 \frac{\partial \Phi_i}{\partial r} U_i) \frac{\partial \Phi_1}{\partial r} & \frac{1}{2}(\sum_{i=1}^4 \frac{\partial \Phi_i}{\partial r} W_i) \frac{\partial \Phi_1}{\partial r} & \dots \\ \frac{1}{2r^2}(\sum_{i=1}^4 \Phi_i U_i) \Phi_1 & 0 & \dots \\ \frac{1}{2}(\sum_{i=1}^4 \frac{\partial \Phi_i}{\partial z} U_i) \frac{\partial \Phi_1}{\partial z} & \frac{1}{2}(\sum_{i=1}^4 \frac{\partial \Phi_i}{\partial z} W_i) \frac{\partial \Phi_1}{\partial z} & \dots \\ (\sum_{i=1}^4 \frac{\partial \Phi_i}{\partial z} U_i) \frac{\partial \Phi_1}{\partial r} & (\sum_{i=1}^4 \frac{\partial \Phi_i}{\partial z} W_i) \frac{\partial \Phi_1}{\partial r} & \dots \\ \frac{1}{2}(\sum_{i=1}^4 \frac{\partial \Phi_i}{\partial r} U_i) \frac{\partial \Phi_4}{\partial r} & \frac{1}{2}(\sum_{i=1}^4 \frac{\partial \Phi_i}{\partial r} W_i) \frac{\partial \Phi_4}{\partial r} & \dots \\ \frac{1}{2r^2}(\sum_{i=1}^4 \Phi_i U_i) \Phi_4 & 0 & \dots \\ \frac{1}{2}(\sum_{i=1}^4 \frac{\partial \Phi_i}{\partial z} U_i) \frac{\partial \Phi_4}{\partial z} & \frac{1}{2}(\sum_{i=1}^4 \frac{\partial \Phi_i}{\partial z} W_i) \frac{\partial \Phi_4}{\partial z} & \dots \\ (\sum_{i=1}^4 \frac{\partial \Phi_i}{\partial z} U_i) \frac{\partial \Phi_4}{\partial r} & (\sum_{i=1}^4 \frac{\partial \Phi_i}{\partial z} W_i) \frac{\partial \Phi_4}{\partial r} & \dots \end{bmatrix} \quad (26)$$

Now by using Hamilton's principle and Rayleigh–Ritz energy formulation, the NGFEM is imposed and finally the stiffness and force matrices are obtained as following:

$$\int_{t_1}^{t_2} \delta(\Pi - W) dt = 0 \quad (27)$$

where  $\Pi$  and  $W$  are potential energy and virtual work done by body forces, respectively. These functions and their variations are:

$$\Pi = \frac{1}{2} \int_{\Omega} \boldsymbol{\varepsilon}^T \boldsymbol{\sigma} d\Omega \quad (28)$$

$$\delta \Pi = \int_{\Omega} \delta \boldsymbol{\varepsilon}^T \boldsymbol{\sigma} d\Omega \quad (29)$$

$$W = \int_{\Omega} \mathbf{P}^T \mathbf{U} d\Omega \quad (30)$$

$$\delta W = \int_{\Omega} \mathbf{P}^T \delta \mathbf{U} d\Omega \quad (31)$$

where  $\Omega$  is the volume of the domain under consideration and  $\mathbf{P}$  is the vector of body forces and in the case of rotating disk is as:

$$\mathbf{P} = \{\rho r \omega^2 \quad 0\}^T \quad (32)$$

Also, it should be mentioned that  $\delta \boldsymbol{\varepsilon} = \tilde{\mathbf{B}} \delta \mathbf{A}$  in which  $\tilde{\mathbf{B}} = \mathbf{B}_L + 2\mathbf{B}_{NL}$ . Substituting Eqs. (28)–(31) in Hamilton's Principle, applying side conditions  $\delta \mathbf{U}|_{t_1, t_2} = 0$  and using part integration give:

$$\int_{\Omega} \delta \boldsymbol{\varepsilon}^T \boldsymbol{\sigma} d\Omega = \int_{\Omega} \mathbf{P}^T \delta \mathbf{U} d\Omega \quad (33)$$

By imposing Eqs. (13), (19) and (25) into Eq. (33) for each element, it can be achieved that:

$$\delta \mathbf{A}^{(e)T} \left\{ \int_{\Omega} \tilde{\mathbf{B}}^T \mathbf{D} \mathbf{B} d\Omega \right\} \mathbf{A}^{(e)} = \delta \mathbf{A}^{(e)T} \int_{\Omega} \Phi^T \mathbf{P} d\Omega \quad (34)$$

Since  $\delta \mathbf{A}^{(e)T}$  is the variation of the nodal displacements and is arbitrary, it can be omitted from Eq. (35). Due to dependency of matrix  $\mathbf{B}$  and  $\tilde{\mathbf{B}}$  to the nodal displacements, the element stiffness matrix becomes a function of nodal displacements. Thus, the nonlinear equations can be formulated as:

$$[\mathbf{K}^{(e)}(\{\mathbf{A}^{(e)}\})] \{\mathbf{A}^{(e)}\} = \{\mathbf{F}^{(e)}\} \quad (35)$$

where the characteristic matrices are defined as:

$$\mathbf{K}^{(e)} = \int_{\Omega} \tilde{\mathbf{B}}^T \mathbf{D} \mathbf{B} d\Omega \quad (36)$$

$$\mathbf{F}^{(e)} = \int_{\Omega} \Phi^T \mathbf{P} d\Omega \quad (37)$$

Now by assembling the element matrices, the global nonlinear equations for the FG-CNTRC rotating disk can be written as:

$$[\mathbf{K}(\{\mathbf{A}\})]\{\mathbf{A}\} = \{\mathbf{F}\} \quad (38)$$

The nonlinear algebraic equations of the problem should be solved by an iterative method. In iterative methods, the nonlinear equations are linearized by evaluating the nonlinear terms with the known solution from preceding iteration(s). Picard method is a commonly used iterative method also known as the direct iteration method. In this method, the solution vector from the previous iteration is used to evaluate the stiffness matrix, and the solution at the subsequent iteration is determined by solving the assembled equations after the imposition of boundary conditions [23]. Accordingly, Eq. (38) may be expressed as:

$$[\mathbf{K}(\{\mathbf{A}^{\kappa}\})]\{\mathbf{A}^{\kappa+1}\} = \{\mathbf{F}\} \quad (39)$$

where  $\{\mathbf{A}^{\kappa}\}$  denotes the solution vector at the  $\kappa$ th iteration. The iteration process begins with an initial guess for displacements vector ( $\{\mathbf{A}^1\}$ ) and determines the next approximation using Eq. (39). This procedure is continued until the difference between  $\{\mathbf{A}^{\kappa}\}$  and  $\{\mathbf{A}^{\kappa+1}\}$  decreases to a preselected error tolerance. The global error criterion is of the form [22]:

$$\sqrt{\frac{\sum_{I=1}^N |\mathbf{A}_I^{\kappa+1} - \mathbf{A}_I^{\kappa}|^2}{\sum_{I=1}^N |\mathbf{A}_I^{\kappa+1}|^2}} < \epsilon \quad (40)$$

where  $\epsilon$  denotes the convergence tolerance and  $N$  is the total number of nodal displacements in the finite element mesh. In the current study, to obtain more accurate results and optimized computational efficiency, the convergence tolerance is taken as  $\epsilon = 10^{-2}$  and the initial guess ( $\{\mathbf{A}^1\}$ ) is assumed to be the linear response of the system.

### 3. Numerical results and discussion

#### 3.1. Validation

To validate the presented work, the data of a functionally graded rotating disk can be used [5]. The inner and outer radii of the disk are  $a = 40$  mm and  $b = 100$  mm, respectively, and the thickness of the disk is small ( $h(r) = \text{const.} = 2.5$  mm). The elasticity modulus and density vary in the  $r$  direction as below:

$$E(r) = E_0(r/b)^n, \quad \rho(r) = \rho_0(r/b)^n \quad (41)$$

where  $E_0 = 72$  GPa,  $\rho_0 = 2800$  kg/m<sup>3</sup> and the angular velocity is  $\omega = 1570.8$  rad/s. The boundary condition is free in both inner and outer surfaces. The comparison of the radial stress along the radial direction for  $n = 0, 0.5, 1$  with the published data is shown in Fig. 3 and a good agreement between these results is observed.

#### 3.2. Numerical results

In this section, the nonlinear response of FG-CNTRC thick rotating disks is presented. The disk is made of Polymethylmethacrylate (PMMA) as matrix, where SWCNTs are act as fibers aligned in radial direction. The properties of basic materials are [11,26]:

$$E^m = 2.5 \text{ GPa}, \quad \nu^m = 0.34, \quad \rho^m = 1150 \text{ kg/m}^3 \quad (42)$$

$$E_1^{CNT} = 5.6466 \text{ TPa}, \quad E_2^{CNT} = 7.08 \text{ TPa}, \\ \nu^m = 0.175, \quad \rho^m = 1400 \text{ kg/m}^3 \quad (43)$$

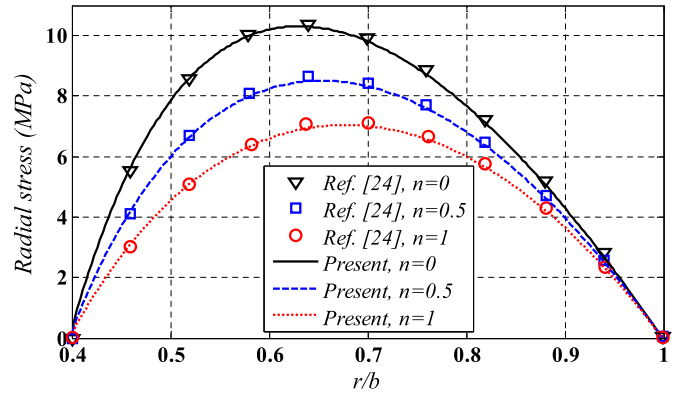


Fig. 3. Radial stress along radial direction compared with [5].

Table 2  
Different types of thickness profiles.

Constant	Linear	Concave	Convex
$q = 0$	$q = 0.7$ $m = 1$	$q = 0.7$ $m = 0.5$	$q = 0.7$ $m = 2$

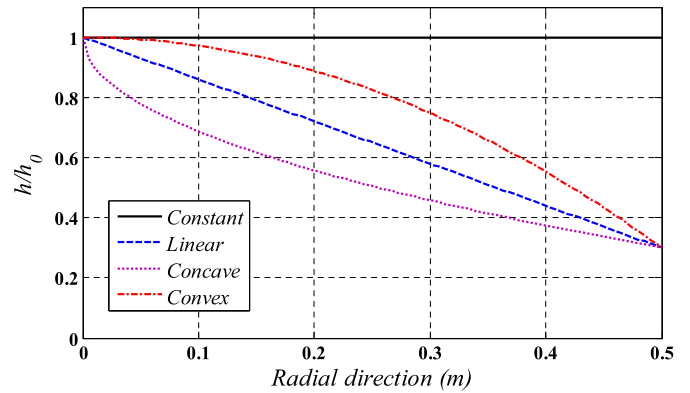


Fig. 4. Different types of thickness profiles.

Furthermore, the thickness profile of FG-CNTRC disk is in the form of:

$$h(r) = h_0[1 - q(r/b)^m] \quad (44)$$

where  $h_0 = b/10$ ,  $q$  and  $m$  are geometric parameters that  $0 \leq q < 1$  and  $m > 0$ . By changing the values of  $q$  and  $m$  four different types of thickness profiles, namely constant, linear, concave and convex are introduced in Table 2 and in the case of  $a = 0$ ,  $b = 0.5$  m are shown in Fig. 4.

The disk rotates about  $z$  axis with an angular velocity of  $\omega$ . The boundary condition of the disk is clamped on its inner surface and free on its outer surface, where:

$$a = 0.1 \text{ m}, \quad b = 0.5 \text{ m}, \quad \omega = 3000 \text{ rad/s} \quad (45)$$

The effects of CNTs' distribution type on the variation of radial displacement and stress and circumferential stress along the radial direction of FG-CNTRC disk, are shown in Figs. 5–7, respectively. The thickness profile and volume fraction of CNTs are assumed to be linear and 0.12, respectively. According to these figures, the FG\_V type of distribution has the largest radial displacement and circumferential stress among the other types, and the radial stress doesn't vary significantly with the types of CNTs' distribution. This behaviour can be explained in more details as follows. According to Eq. (13) and the fact that  $D_{11} > D_{12}$ , it can be concluded that  $\sigma_r$  is mostly dependent on  $\epsilon_r$  and Eq. (18) shows that  $\epsilon_r$  is a

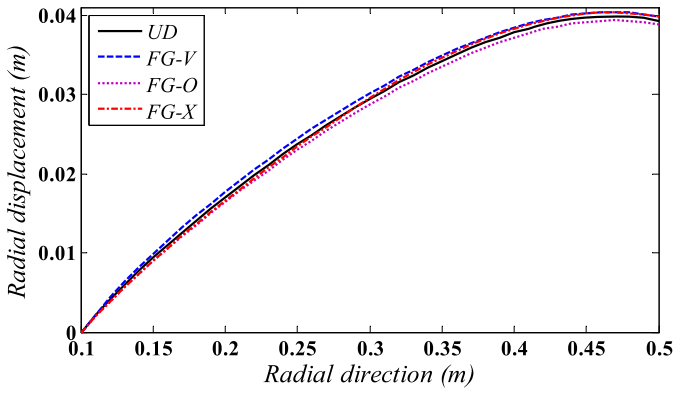


Fig. 5. Variation of radial displacement along radial direction of disk with linear profile and  $V_{CNT}^* = 0.12$ .

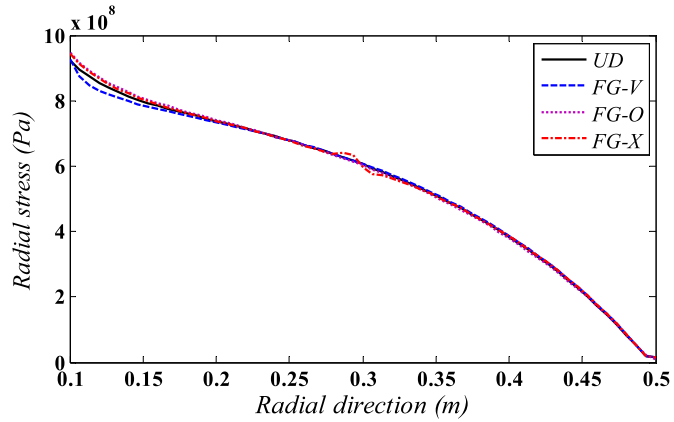


Fig. 6. Variation of radial stress along radial direction of disk with linear profile and  $V_{CNT}^* = 0.12$ .

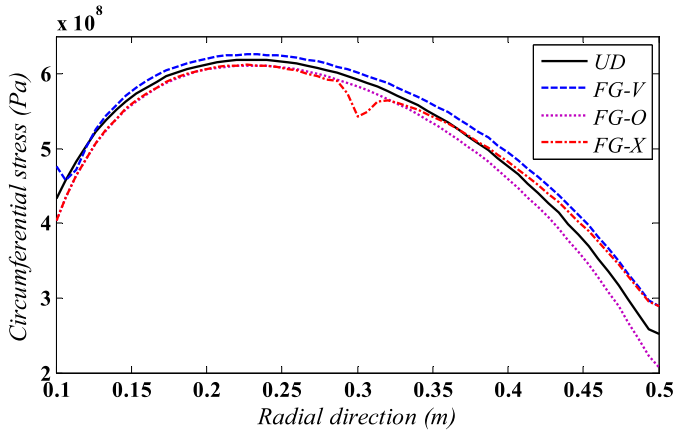


Fig. 7. Variation of circumferential stress along radial direction of disk with linear profile and  $V_{CNT}^* = 0.12$ .

function of  $\partial u/\partial r$ . Now, as it is seen from Fig. 5, when the radial displacement ( $u$ ) varies, its slope ( $\partial u/\partial r$ ) doesn't vary considerably for different CNTs' distribution types, which causes to have nearly the same radial stresses for different distributions.

Moreover, in FG\_X type of distribution, at  $r = 0.3$  m according to Eq. (9), the volume fraction of CNTs vanishes. Hence, at this radius the disk is consisted of homogeneous and isotropic material and as a result, a jump in the material properties is occurred at this radius ( $r_m$ ) which yields to a discontinuity in stress field.

The variations of radial displacement and stress and circumferential stress along the radial direction of FG-CNTRC disk for

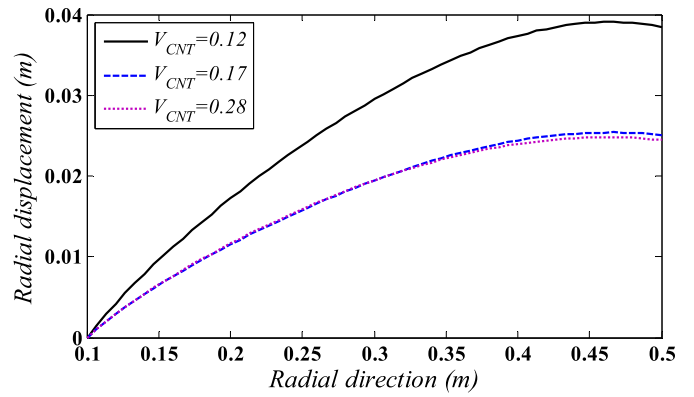


Fig. 8. Variation of radial displacement along radial direction of disk with concave profile and FG\_V type of distribution.

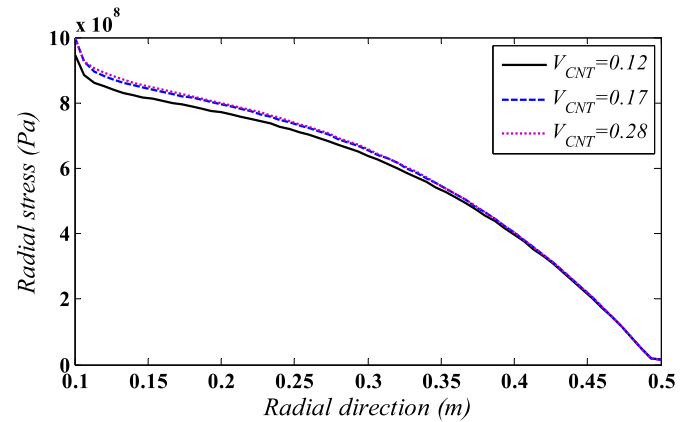


Fig. 9. Variation of radial stress along radial direction of disk with concave profile and FG\_V type of distribution.

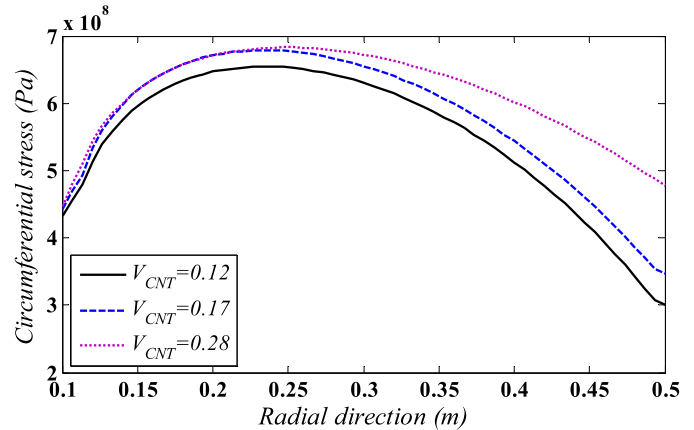


Fig. 10. Variation of circumferential stress along radial direction of disk with concave profile and FG\_V type of distribution.

different volume fractions of CNTs, are illustrated in Figs. 8–10, respectively. In this case, the thickness profile is concave and the type of distribution is FG\_V type. As it can be seen, when volume fraction of CNTs rises, due to growth of structural stiffness, the radial displacement decreases while the radial and circumferential stresses increase.

Figs. 11–13 depict the influence of thickness profile on the variations of radial displacement and stress and circumferential stress along the radial direction of FG-CNTRC disk, respectively. The type of distribution and volume fraction of CNTs are assumed to be FG\_O type and 0.17, respectively. It is obvious that by utilizing

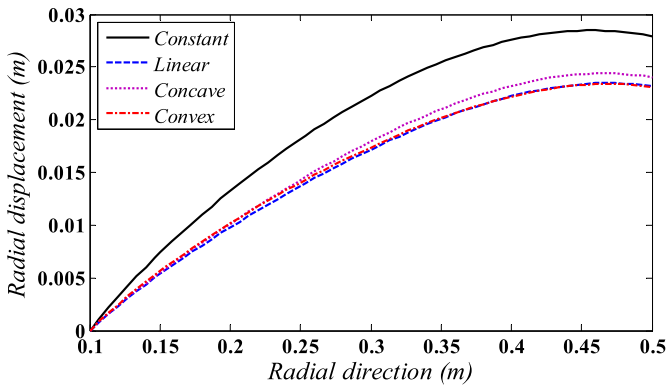


Fig. 11. Variation of radial displacement along radial direction of disk with  $V_{CNT}^* = 0.17$  and FG\_O type of distribution.

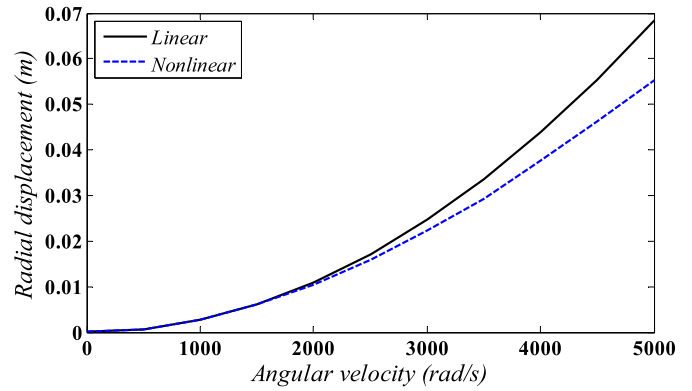


Fig. 14. Variation of radial displacement versus angular velocity in two cases of linear and nonlinear analyses.

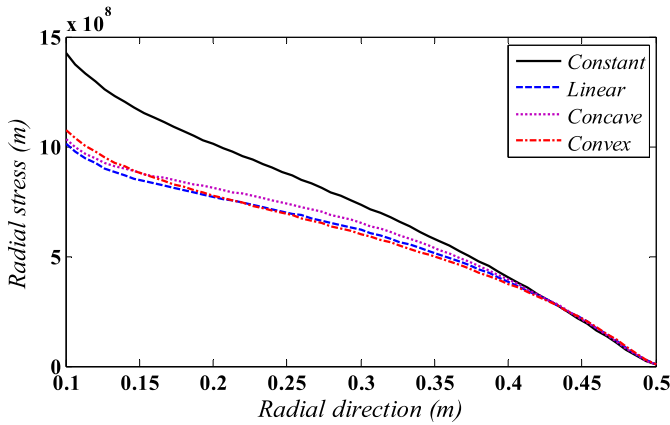


Fig. 12. Variation of radial stress along radial direction of disk with  $V_{CNT}^* = 0.17$  and FG\_O type of distribution.

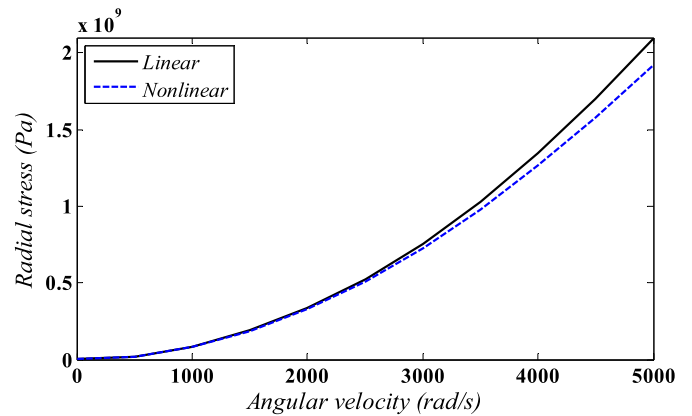


Fig. 15. Variation of radial stress versus angular velocity in two cases of linear and nonlinear analyses.

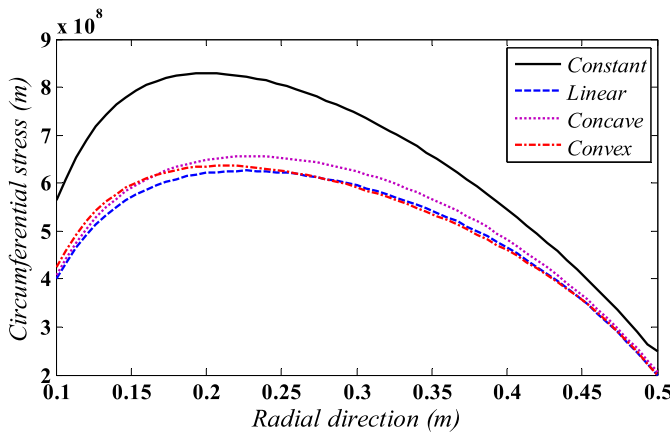


Fig. 13. Variation of circumferential stress along radial direction of disk with  $V_{CNT}^* = 0.17$  and FG\_O type of distribution.

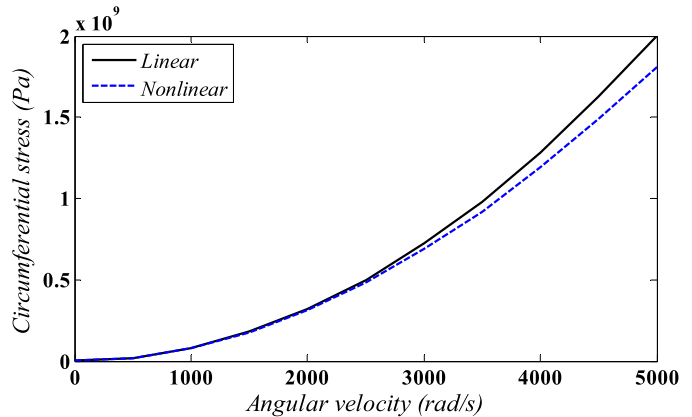


Fig. 16. Variation of circumferential stress versus angular velocity in two cases of linear and nonlinear analyses.

variable thickness, the displacement and stress fields are affected significantly, hence a capability of higher  $\omega$  can be reached.

The comparison between linear and nonlinear responses of radial displacement and stress and circumferential stress at  $r = 0.3$  m and  $z = 0$  m versus angular velocity ( $\omega$ ) are demonstrated in Figs. 14–16, respectively. In this case, the thickness profile is constant and the type of distribution and volume fraction of CNTs are FG\_X type and 0.28, respectively. According to these figures, as the angular velocity grows, the effect of geometric nonlinearity becomes more noticeable and the difference between linear and nonlinear responses increases considerably. Thus, in high angular

velocities, in order to obtain accurate results, the geometric nonlinearity must be considered.

#### 4. Conclusions

The main purpose of the present paper was to investigate the nonlinear elasticity behaviour of FG-CNTRC rotating thick disks with variable thickness. The nonlinear graded finite element method based on Rayleigh–Ritz energy formulation with Picard iteration method is applied. For the sake of validation, a functionally graded rotating annular disk with available solution in the published literature was taken into consideration and stresses were

presented for various values of power law exponents. The comparisons between the obtained results and the literature showed a good agreement. Various types of displacements and stresses are presented for different types of distributions and volume fractions of CNTs as well as different types of thickness profiles of rotating disks. Based on the achieved results, FG\_CNTRCs have powerful potentials for designing and optimizing structures under functional requirements and a higher  $\omega$  can be reached by utilizing variable thickness. Moreover, results demonstrate that in high angular velocities, the effect of nonlinearity is remarkable where the nonlinear displacements and stresses are smaller than linear ones.

### Conflict of interest statement

Authors certify that there is not any conflict of interest.

### References

- [1] M. Asghari, E.A. Ghafoori, Three-dimensional elasticity solution for functionally graded rotating disks, *Compos. Struct.* 92 (2010) 1092–1099.
- [2] H. Ashrafi, K. Asemi, M. Shariyat, M. Salehi, Two dimensional modelling of heterogeneous structures using graded finite element and boundary element methods, *Meccanica* 48 (2012) 663–680.
- [3] M. Bayat, M. Saleem, B.B. Sahari, A.M.S. Hamouda, E. Mahdi, Thermo elastic analysis of a functionally graded rotating disk with small and large deflections, *Thin-Walled Struct.* 45 (2007) 677–691.
- [4] A.P. Boresi, K.P. Chong, J.D. Lee, *Elasticity in Engineering Mechanics*, third ed., John Wiley Sons, Inc., Hoboken, New Jersey, 2011.
- [5] H. Callioglou, N.B. Bektas, M. Sayer, Stress analysis of functionally graded rotating discs, analytical and numerical solutions, *Acta Mech. Sin.* 27 (2011) 950–955.
- [6] H. Dai, Carbon nanotubes: opportunities and challenges, *Surf. Sci.* 500 (2002) 218–241.
- [7] J.F. Durodola, O. Attia, Deformation and stresses in FG rotating disks, *Compos. Sci. Technol.* 60 (2000) 987–995.
- [8] A.M.K. Esawi, M.M. Farag, Carbon nanotube reinforced composites: potential and current challenges, *Mater. Des.* 28 (2007) 2394–2401.
- [9] B. Fiedler, F.H. Gojny, M.H.G. Wichmann, M.C.M. Nolte, K. Schulte, Fundamental aspects of nano-reinforced composites, *Compos. Sci. Technol.* 66 (2006) 3115–3125.
- [10] M.E. Golmakani, Large deflection thermoelastic analysis of shear deformable functionally graded variable thickness rotating disk, *Composites, Part B, Eng.* 45 (2013) 1143–1155.
- [11] Y. Han, J. Elliott, Molecular dynamics simulations of the elastic properties of polymer/carbon nanotube composites, *Comput. Mater. Sci.* 39 (2007) 315–323.
- [12] N. Hu, H. Fukunaga, C. Lu, M. Kameyama, B. Yan, Prediction of elastic properties of carbon nanotube reinforced composites, *Proc. R. Soc. A, Math. Phys. Eng. Sci.* 461 (2005) 1685–1710.
- [13] I. Kang, Y. Heung, J. Kim, J. Lee, R. Gollapudi, S. Subramaniam, S. Narasimhadvara, D. Hurd, G.R. Kiriker, V. Shanov, M.J. Schulz, D. Shi, J. Boerio, S. Mall, M. Ruggles-Wren, *Introduction to carbon nanotube and nanofiber smart materials*, *Composites, Part B, Eng.* 37 (2006) 382–394.
- [14] J.H. Kim, G.H. Paulino, Isoparametric graded finite elements for nonhomogeneous isotropic and orthotropic materials, *Int. J. Appl. Mech.* 69 (2002) 502–514.
- [15] M. Koizumi, The concept of FGM, in: *Functionally Graded Materials*, in: *Ceramic Transactions*, vol. 34, 1993, pp. 3–10.
- [16] S.A.H. Kordkheili, R. Naghdabadi, Thermo-elastic analysis of a functionally graded rotating disk, *Compos. Struct.* 79 (2007) 508–516.
- [17] K.T. Lau, C. Gu, D. Hui, A critical review on nanotube and nanotube/nanoclay related polymer composite materials, *Composites, Part B, Eng.* 37 (2006) 425–436.
- [18] M. Moradi-Dastjerdi, A. Pourasghar, M. Foroutan, M. Bidram, Vibration analysis of functionally graded nanocomposite cylinders reinforced by wavy carbon nanotube based on mesh-free method, *J. Compos. Mater.* 48 (2014) 1901–1913.
- [19] G.J. Nie, R.C. Batra, Stress analysis and material tailoring in isotropic linear thermoelastic incompressible functionally graded rotating disks of variable thickness, *Compos. Struct.* 92 (2010) 720–729.
- [20] G.M. Odegard, T.S. Gates, L.M. Nicholson, K.E. Wise, Equivalent-continuum modeling of nano-structured materials, *Compos. Sci. Technol.* 62 (2002) 1869–1880.
- [21] G.M. Odegard, T.S. Gates, K.E. Wise, C. Park, E.J. Siochi, Constitutive modeling of nanotube-reinforced polymer composites, *Compos. Sci. Technol.* 63 (2003) 1671–1687.
- [22] J.N. Reddy, Analysis of functionally graded plates, *Int. J. Numer. Methods Eng.* 47 (2000) 663–684.
- [23] J.N. Reddy, *An Introduction to Nonlinear Finite Element Analysis*, Oxford University Press Inc., New York, 2004.
- [24] J.N. Reddy, *Mechanics of Laminated Composite Plates and Shells, Theory and Analysis*, second edition, CRC Press LLC, Boca Raton, Florida, 2011.
- [25] M. Shariyat, R. Mohammadjani, Three-dimensional stress field analysis of rotating thick bidirectional functionally graded axisymmetric annular plates with non-uniform loads and elastic foundations, *J. Compos. Mater.* (2013), <http://dx.doi.org/10.1177/0021998313503389>.
- [26] H.S. Shen, Nonlinear bending of functionally graded carbon nanotube reinforced composite plates in thermal environments, *Compos. Struct.* 91 (2009) 9–19.
- [27] H.S. Shen, Postbuckling of nanotube-reinforced composite cylindrical shells in thermal environments. Part II: Pressure-loaded shells, *Compos. Struct.* 93 (2011) 2496–2503.
- [28] B. Sobhani Aragh, M.H. Yas, Static and free vibration analyses of continuously graded fiber-reinforced cylindrical shells using generalized power-law distribution, *Acta Mech.* 215 (2010) 155–173.
- [29] E.T. Thostenson, Z.F. Ren, T.W. Chou, Advances in the science and technology of carbon nanotubes and their composites: a review, *Compos. Sci. Technol.* 61 (2001) 1899–1912.
- [30] M.H. Yas, A. Pourasghar, S. Kamarian, M. Heshmati, Three-dimensional free vibration analysis of functionally graded nanocomposite cylindrical panels reinforced by carbon nanotube, *Mater. Des.* 49 (2013) 583–590.
- [31] H. Zafarmand, B. Hassani, Analysis of two-dimensional functionally graded rotating disks with variable thickness, *Acta Mech.* 225 (2014) 453–464.
- [32] H. Zafarmand, M. Kadkhodayan, Three-dimensional static analysis of thick functionally graded plates using graded finite element method, in: *Proceedings of the Institution of Mechanical Engineers, Part C, J. Mech. Eng. Sci.* 228 (2014) 1275–1285.
- [33] A.M. Zenkour, Analytical solutions for rotating exponentially-graded annular disks with various boundary conditions, *Int. J. Struct. Stab. Dyn.* 5 (2005) 557–577.
- [34] A.M. Zenkour, D.S. Mashat, Analytical and numerical solutions for a rotating annular disk of variable thickness, *Appl. Math.* 1 (2010) 431–438.
- [35] P. Zhu, Z.X. Lei, K.M. Liew, Static and free vibration analyses of carbon nanotube reinforced composite plates using finite element method with first order shear deformation plate theory, *Compos. Struct.* 94 (2012) 1450–1460.
- [36] R. Zhu, E. Pan, A.K. Roy, Molecular dynamics study of the stress-strain behavior of carbon-nanotube reinforced Epon 862 composites, *Mater. Sci. Eng. A, Struct. Mater.: Prop. Microstruct. Process.* 447 (2007) 51–57.